Supplementary Information

High-Speed Liquid Switching and On-Chip Force Sensing Reveal the Transient Mechanical Response of MscL in *Synechocystis* sp. PCC 6803

Xu Du[1,2], Masaru Tsujii[3], Nobuyuki Uozumi[3] and Fumihito Arai[2,4]*

1. Key Laboratory of Intelligent Flexible Actuation and Control in Universities of Jiangsu Province and School of Mechanical Engineering, Jiangsu University, Zhenjiang 212003, China

2. Department of Micro-Nano Mechanical Science and Engineering, Nagoya University, Nagoya 464-8603, Japan

3. Department of Biomolecular Engineering, Graduate School of Engineering, Tohoku University, Sendai 980-8579, Japan

4. Department of Mechanical Engineering, The University of Tokyo, Tokyo 113-8656, Japan

1. Equipment

The 3D-printed probe was fabricated in two parts due to the size limitation of the high-resolution printer. The probe tip was printed using a high-precision 3D printer (BMF 130, BMF Precision Tech Inc., China), while the connector part was fabricated using a 3D printer with a larger build volume (Foto 6.0, Zhejiang Flashforge 3D Technology Co., Ltd., China) and assembled using adhesive. Solution injection into the liquid switching module was performed using a syringe pump (KDS120, KD Scientific Inc., USA). The liquid switching module was positioned near the chip surface using a 3D micromanipulator (SMX, Sensapex, Finland). The single cell on the chip was trapped at the focal point of the laser (Yb fiber laser, IPG Photonics, wavelength: 1064 nm), and transported by controlling the focal point position via Galvano mirrors (GVS102, Thorlabs Japan Inc., Japan). Local liquid switching and probe motion were recorded using a high-speed camera (VW-9000, KEYENCE CORPORATION, Japan) at 1000 fps.

2. Chip fabrication

An open-type microfluidic chip (3 cm × 3 cm) was used in this work.[1] The chip consists of a 100 μm-thick cover glass bonded to a silicon-on-insulator (SOI) wafer, which includes a 10 μm device layer and a 400 μm handle layer. The use of a thinner device layer enables higher sensitivity in the sensing structure and ensures better compatibility with the size of the target cells. To ensure compatibility with the liquid switching probe and allow real-time observation, the chip was designed without a top sealing layer, forming an open microfluidic structure. The pushing probe was embedded within the device layer to avoid fluid leakage. The final chip layout includes four identical pairs of on-chip probes per chip. The fabrication process is shown below:

Glass: Spin-coat and pattern SU-8 3010 (Nihon Kayaku Co. Ltd, Gumma, Japan). Etch the glass by DRIE to make shallow grooves (Figure S1A). Sputter a thin Cr film on the grooved area to prevent adhesion. Remove SU-8 with piranha.

Device layer (~10 μm): Spin-coat and pattern OFPR (Tokyo Ohka Co., Ltd., Tokyo, Japan). Etch the device layer by DRIE to form the probe. Remove the resist with Piranha (Figure S1B).

Bonding: Bond the processed glass to the SOI device layer.

Handle layer (~400 μm): Spin-coat and pattern SU-8 (Figure S1C). Etch the handle layer by DRIE. Remove SU-8 with oxygen plasma.

Final: Remove the Cr with a chrome etchant.

The fabricated microfluidic chip is shown in Figure S1D.

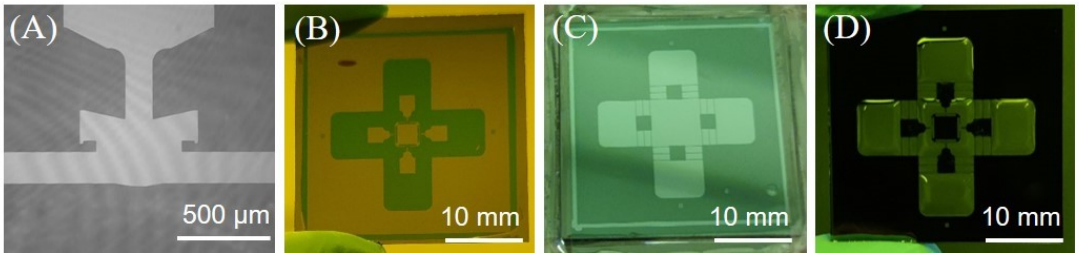

Figure S1. Fabrication process and optical images of the microfluidic chip. (A) Etched glass layer. (B) Etched device layer. (C) Developed handle layer. (D) Fabricated microfluidic chip.

3. Force detection and calibration

Force measurement on the microfluidic chip was achieved using an on-chip force sensor fabricated by etching the device layer of an SOI wafer. The sensor comprises a hollow folded-beam structure connected to a movable probe. This configuration is used to obtain near translational motion of the probe tip with reduced angular rotation, and to keep a long linear displacement range during bending. In our design, the hollow folded beam can be viewed as two serial beams in parallel, providing a low spring constant while maintaining structural symmetry and stable in plane deflection during liquid switching. The dimensions of a single beam segment are L = 1000 μm, w = 5 μm, and h = 10 μm. The parallel gap of the folded beam is 60 μm, which defines the maximum probe displacement without mechanical interference. The pushing probe is driven by an external piezo actuator. When it compresses a target bead or cell against the sensor probe, the folded beam deflects. This deflection corresponds to the reactive force acting on the single cell. This bending-based detection method enables real-time mechanical characterization in liquid environments and allows direct optical observation of probe displacement. Probe displacement was measured using a sampling moiré method. Periodic micro-patterns fabricated on the probe tips produced moiré fringes under the microscope, and the displacement was quantified by analyzing the phase shift of the fringes.[2]

In addition, the cell did not contact the underlying glass substrate during measurement. The device layer thickness (~10 μm) is significantly larger than the cell diameter (~2 μm), ensuring that the cell remained suspended between the probes. The glass beneath the probe region was etched during fabrication to reduce potential contact. And cells were centrifuged at 620× g for 5 min and resuspended prior to measurement to reduce extracellular polysaccharides[3,4]. In some cases, after compression and probe retraction, the cell temporarily adhered to one probe. However, no elastic rebound or sudden displacement jump of the sensing beam was observed during separation. After separation, the cell could be released.

The spring constant k of the folded-beam structure was first estimated analytically as: [5]

$$k = w^3 h E_b / L^3 \tag{1}$$

Where E_b is the Young's modulus of silicon, and L, w, and h denote the length, width, and thickness of the rectangular beam.

For experimental calibration, polydimethylsiloxane (PDMS) beads with a known Young's modulus and a Poisson's ratio *v* of 0.5 were employed. PDMS (SILPOT 184; DuPont Toray, Japan) was mixed at a base to curing agent ratio of 10:1. The PDMS microspheres and PDMS bars were fabricated from the same material under identical conditions, yielding nearly identical Young's modulus values. The Young's modulus of the PDMS bar was measured using a load sensor (LVS-10GA, Kyowa Electronic Instruments Co., Ltd., Japan) (Figure S2A). To minimize the influence of initial curing effects, the measurements were performed starting one to two weeks after fabrication and continued for five consecutive days, giving a Young's modulus of 1.20 ± 0.05 MPa. The averaged value was then adopted as the Young's modulus of the PDMS microspheres.

The relationship between the spring constant k of the force sensor and the Young's modulus E_c of the PDMS beads can be expressed by the Hertz model for non-adhesive elastic spheres: [6]

$$F = k\delta_s = \frac{4(D_0/2)^{1/2}}{3} \cdot \frac{E_c}{1-\nu^2} \cdot \left(\frac{\delta_c}{2}\right)^{3/2} \tag{2}$$

Where F is the applied force, δ_s is the displacement of the sensor probe, δ_c and D_0 is the initial diameter of beads. By fitting the measured deflection of the sensor probe to the theoretical Hertz curve, the spring constant was calibrated (Figure S2B and C).[1] The same measurement principle as used for PDMS beads was applied to the single-cell Young's modulus measurement.

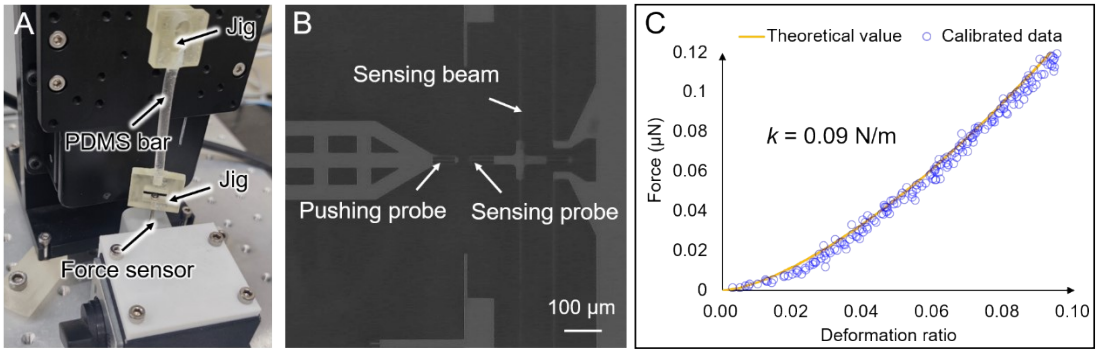

Figure S2. Calibration of the spring constant of the sensing beam. (A) Experimental setup for the measurement of the PDMS bar. (B) Image of the on-chip probes and sensing beam. (C) Example of calibrating the spring constant of the sensing beam, where the measured force–deformation data were fitted to the theoretical Hertz model.

The maximum displacement of the sensing probe is limited by the 60 μm parallel gap of the folded-beam structure. Since this value is smaller than the estimated linear deformation limit of the beam (~10% of the 1000 μm beam length), the accessible displacement range under linear operation is 0–60 μm. With a calibrated spring constant of 0.076 ± 0.018 N m^{-1}, the corresponding accessible force range is approximately 0–4.56 μN.

The force is calculated from the displacement of the sensing probe. The displacement noise was recorded for 0.5 s under experimental conditions, and the stability was quantified using 3σ of the displacement signal. This corresponds to a force resolution of approximately 3.10 nN.[1]

In addition, based on a lumped mass–spring approximation, the characteristic frequency of the folded-beam sensing structure is estimated to be on the order of kHz. The dynamic response was further evaluated experimentally by deflecting the sensing beam with the piezo-driven pushing probe and rapidly releasing it. The recovery motion was recorded at 1000 fps. The sensing probe returned to equilibrium within 1 ms, and no obvious ringing was observed. This indicates that the mechanical response time of the sensor is shorter than 1 ms. In the present study, all measurements were performed at timescales longer than the sensor response time; therefore, the sensor bandwidth does not limit the reported results.

4. Response time of the liquid switching module

Achieving millisecond-scale liquid switching is essential for analyzing transient mechanical responses of cells under dynamic conditions. Although the piezoelectric actuator itself can respond on a microsecond scale, the overall liquid switching speed is limited by fluid inertia, elastic deformation of the deformation segment, and hydraulic resistance in the microchannel. The dynamic response of the liquid switching process can be described as a second-order mass–spring–damper system:

$$m\frac{d^2x}{dt^2} + c\frac{dx}{dt} + kx = F(t) \tag{3}$$

Here, *m* denotes the effective mass of fluid in the microchannel, *c* is the viscous damping, *k* is the spring constant of the deformation segment, and *F(t)* is the external driving force produced by the piezo actuator. Following the standard hydraulic–mechanical analogy, the inertial, resistive, and compliant behaviors of the fluidic system are treated as the mechanical counterparts of mass, damping, and spring stiffness, thereby forming a second-order dynamic model. And the effective fluid mass can also be written as:

$$m = \alpha\rho\pi r^2 L \tag{4}$$

Where ρ is the fluid density, r and L are the radius and length of the main flow channel, respectively, and $\alpha = 2$ is a kinetic energy correction factor accounting for the parabolic velocity profile in fully developed Poiseuille flow. [7]

The stiffness k represents the overall elastic response of the fluidic system. Because the liquid and glass capillary components are nearly rigid, deformation occurs primarily in the deformation segment (silicone tube). Thus, the total stiffness is dominated by the stiffness of the deformation segment.

Considering that the deformation segment is a short and thick-walled cylinder, its spring constant k is evaluated using the Lamé solution for a thick-walled cylinder with closed-end boundary conditions. The corresponding volumetric stiffness k_{vol} of the tube can be expressed as:[8]

$$k_{vol} = \frac{E}{2\pi r_i^2 L_e} \frac{b^2 - r_i^2}{(1 - \nu - 2\nu^2)\, r_i^2 + (1 + \nu)\, b^2} \tag{5}$$

Where E and ν are the Young's modulus and Poisson's ratio of the deformation segment; r_i and

b are the inner and outer radii; L_e is the effective deformation length of the tube.

The acceleration-dominated behavior can be characterized by the inertial time constant:

$$\tau_d = \sqrt{\frac{m}{k}} = \sqrt{\frac{\alpha \rho L}{\pi r^2 k_{vol}}} \tag{6}$$

The spring constant $k = k_{vol} \pi^2 r^4$. This equation shows that the inertial time constant τ_d increases with the channel length L and fluid density ρ, and decreases with the channel radius r and spring constant k. Hence, shortening the flow path or increasing the stiffness of the deformation segment accelerates the liquid switching process.

In terms of the viscous time constant, the viscous damping coefficient c is dominated by the total hydraulic resistance. By substituting structural parameters and comparing each segment along the flow path, it is found that the probe tip contributes the most to the overall resistance due to the extremely small outlet radius (25 μm). The probe tip consists of both a conical and a short cylindrical segment, which are designed to maximize the internal flow radius while avoiding interference between the 3D-printed probe tip and the on-chip structures. Although the cylindrical segment is relatively short, its contribution to flow resistance remains significant because of the fourth-power inverse dependence on the radius. Accordingly, the overall viscous damping R can be estimated as the combined resistance of the conical and cylindrical segments R_{tip}:

$$R_{tip} = \frac{8\mu}{\pi}[L_{cyl} r_2^{-4} + \frac{L_{con}(r_1^3 - r_2^3)}{3 r_1^3 r_2^3 (r_1 - r_2)}] \tag{7}$$

Here, μ is the dynamic viscosity, $L_{con}$and L_{cyl} are the lengths of the conical and cylindrical segments, $r_1$and r_2 are the maximum and minimum radii of the conical tip, respectively. To describe the viscous-dominated response, the viscous time constant can be defined as:

$$\tau_v = \frac{c}{k} \approx \frac{R_{\text{tip}}}{k_{vol}} = \frac{8\,\mu}{\pi k_{vol}} [L_{\text{cyl}} r_2^{-4} + \frac{L_{\text{con}}\,(r_1^3 - r_2^3)}{3\, r_1^3 r_2^3 (r_1 - r_2)}] \tag{8}$$

Since the hydraulic resistance R_{tip} is inversely proportional to the fourth power of the outlet radius $r_2$and increases approximately linearly with the lengths of both the cylindrical and conical segments, by increasing the outlet radius or reducing the tip length, the overall hydraulic resistance can be decreased, thereby shortening the viscous time constant and accelerating the response time.

This section presents the dynamic model of the liquid switching module and defines the

characteristic time constants used to interpret the experimentally measured liquid switching time discussed in the main text.

5. Cell culture and preparation

We selected the model cyanobacterium *Synechocystis sp.* PCC 6803 as the experimental organism. To investigate the mechanistic basis of MS channels, both the wild-type (WT) strain and a mutant strain deficient in the MscL channel (ΔmscL) were used. The ΔmscL strain was constructed by inserting a spectinomycin resistance gene into the *symscL* locus, which encodes a putative large-conductance mechanosensitive channel homolog (*slr0875)*.

WT and ΔmscL cells were cultured in BG11 medium at 28 °C for 5 days under continuous illumination from a 3.5 W white-light LED. Cells were harvested by centrifugation at 620 × g for 2 min to remove extracellular polysaccharides and reduce nonspecific adhesion. Osmotic pressure was controlled by varying the concentration of D-sorbitol (≥98%, S1876, Sigma-Aldrich, France). For liquid switching, the hyperosmotic solution was BG11 containing 0.5 mol L^{-1} D-sorbitol, and the hypoosmotic solution was pure BG11. The osmolarities of the solutions were measured using a freezing-point osmometer (FM-8C, Shanghai Feiyu Biotechnology Co., Ltd.). The osmolarity was 38 mOsm L^{-1} for pure BG11 and 545 mOsm L^{-1} for BG11 containing 0.5 mol L^{-1} D-sorbitol. To visualize the liquid–liquid interface during switching, Rhodamine B (10 g/L) was added (Figure S3).

Cell viability was evaluated using SYTO 9 and propidium iodide (PI) (Life Technologies, USA). SYTO 9 is a green fluorescent dye that penetrates live and dead cells, whereas PI is a red fluorescent dye that enters cells with compromised membranes. PI quenches SYTO 9 fluorescence in damaged cells. Thus, viable cells with intact membranes appear green, while non-viable, membrane-damaged cells fluoresce red.

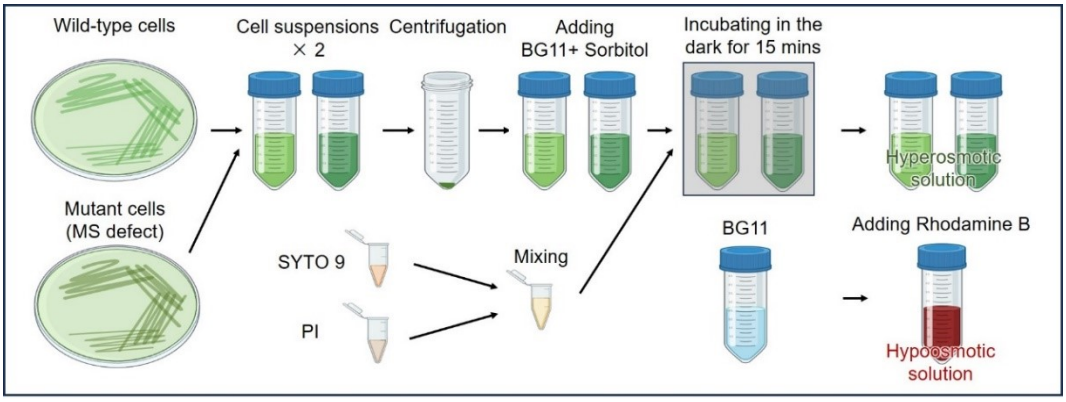

Figure S3. Cell preparation process

The staining protocol was conducted as follows:

(1) Equal volumes of SYTO 9 and PI were mixed in a microcentrifuge tube.

(2) 3 μL of the dye mixture was added to each 1 mL of bacterial suspension.

(3) The samples were incubated in the dark at room temperature for 15 minutes.

Stained cells were observed using a fluorescence microscope equipped with a 470 nm excitation filter. Only green-fluorescent (viable) cells were included in subsequent mechanical measurements, while red-fluorescent cells were excluded from analysis.

References

[1] Du, X.; Kaneko, S.; Maruyama, H.; Sugiura, H.; Tsujii, M.; Uozumi, N.; Arai, F. Integration of Microfluidic Chip and Probe with a Dual Pump System for Measurement of Single Cells Transient Response. *Micromachines* **2023**, *14* (6), 1210.

[2] Sugiura, H.; Sakuma, S.; Kaneko, M.; Arai, F. Large Indentation Method to Measure Elasticity of Cell in Robot-Integrated Microfluidic Chip. *IEEE Robot. Autom. Lett.* **2017**, *2* (4), 2002–2007.

[3] Stuart, R. K.; Mayali, X.; Lee, J. Z.; Craig Everroad, R.; Hwang, M.; Bebout, B. M.; ... & Thelen, M. P. Cyanobacterial reuse of extracellular organic carbon in microbial mats. *The ISME journal* **2016**, *10*(5), 1240-1251.

[4] Bell, C. H. The effects of centrifugation and filtration as pre-treatement in bacterial retention studies. *Journal of Young Investigators* **2005**.

[5] Albrecht, T. R.; Akamine, S.; Carver, T. E.; Quate, C. F. Microfabrication of cantilever styli for the atomic force microscope. *J. Vac. Sci. Technol. A Vac. Surf. Films* **1990**, *8* (4), 3386–3396.

[6] Chang, D.; Sakuma, S.; Kera, K.; Uozumi, N.; Arai, F. Measurement of the mechanical properties of single Synechocystis sp strain PCC6803 cells in different osmotic concentrations using a robot-integrated microfluidic chip. *Lab Chip* **2018**, *18* (8), 1241–1249.

[7] Wang, J.; Geng, J.; Li, D.; Wang, X. The Analysis of Flow Stability in Pipe by Experiment. In *International Symposium on Energy Science and Chemical Engineering (ISESCE)*, Guangzhou, 2016; pp 247–250.

[8] Timoshenko, S. P.; Goodier, J. N. *Theory of Elasticity*, 3rd ed.; McGraw-Hill, 1970.